The Astrophysical Journal Letters, 758:L40 (5pp), 2012 October 20 doi:10.1088/2041-8205/758/2/L40


# RESOLVING THE INTERNAL MAGNETIC STRUCTURE OF THE SOLAR NETWORK

M. J. Martínez González[1,2], L. R. Bellot Rubio[3], S. K. Solanki[4,5], V. Martínez Pillet[1,2], J. C. Del Toro Iniesta[3], P. Barthol[4], and W. Schmidt[6]

[1] Instituto de Astrofísica de Canarias, Vía Láctea s/n, E-38205 La Laguna, Tenerife, Spain
[2] Departamento de Astrofísica, Universidad de La Laguna, E-38205 La Laguna, Tenerife, Spain
[3] Instituto de Astrofísica de Andalucía (CSIC), Apdo. de Correos 3004, E-18080 Granada, Spain
[4] Max-Planck-Institut für Sonnensystemforschung, D-37191 Katlenburg-Lindau, Germany
[5] School of Space Research, Kyung Hee University, Yongin, Gyeonggi 446-701, Republic of Korea
[6] KIS Kiepenheuer-Institut für Sonnenphysik, D-79104 Freiburg, Germany
*Received 2012 July 30; accepted 2012 September 11; published 2012 October 4*

## ABSTRACT

We analyze the spectral asymmetry of Stokes *V* (circularly polarized) profiles of an individual network patch in the quiet Sun observed by Sunrise/IMaX. At a spatial resolution of 0.″15–0.″18, the network elements contain substructure which is revealed by the spatial distribution of Stokes *V* asymmetries. The area asymmetry between the red and blue lobes of Stokes *V* increases from nearly zero at the core of the structure to values close to unity at its edges (single-lobed profiles). Such a distribution of the area asymmetry is consistent with magnetic fields expanding with height, i.e., an expanding magnetic canopy (which is required to fulfill pressure balance and flux conservation in the solar atmosphere). Inversion of the Stokes *I* and *V* profiles of the patch confirms this picture, revealing a decreasing field strength and increasing height of the canopy base from the core to the periphery of the network patch. However, the non-roundish shape of the structure and the presence of negative area and amplitude asymmetries reveal that the scenario is more complex than a canonical flux tube expanding with height surrounded by downflows.

*Key words:* polarization – Sun: atmosphere – Sun: surface magnetism

*Online-only material:* color figures

## 1. INTRODUCTION

Asymmetries in spectral profiles of Stokes *V* are commonly measured on the solar surface, from the penumbrae of sunspots to the quiet Sun, and have been known about for decades (e.g., Solanki & Stenflo 1984; Grossmann-Doerth et al. 1996; Martínez Pillet et al. 1997; Sigwarth 2000, 2001; Rezaei et al. 2007; Martínez González et al. 2008; Viticchié & Sánchez Almeida 2011). The generally accepted model to produce asymmetric Stokes *V* profiles is by having anticorrelated velocity and magnetic field gradients along the line of sight (Illing et al. 1975; Sánchez Almeida et al. 1989; López Ariste 2002). Therefore, circular polarization asymmetries encode the structuring of magnetic fields along the line of sight. However, the limited spatial resolution of most observations mixes the contributions of different regions to the asymmetries, hence allowing only indirect inferences of gradients along the line of sight.

Outside of sunspots the classical model to produce asymmetries is at the canopies of the magnetic features expanding with height (Grossmann-Doerth et al. 1988; Solanki 1989). This model has been able to reproduce the simultaneous presence of Stokes *V* area asymmetry, the absence of a Stokes *V* zero-crossing shift (Solanki 1986; Martínez Pillet et al. 1997), and the change in sign of the area asymmetry near the solar limb (Bünte et al. 1993) in observations of the quiet Sun and active region plage taken at rather low spatial resolution (Stenflo et al. 1987; Martínez Pillet et al. 1997). Alternatives have also been suggested, such as the presence of bulk velocities in the flux tube (Bellot Rubio et al. 1997a, 1997b; Sigwarth 2001), or the MISMA and MESMA models (Sánchez Almeida & Landi Degl'Innocenti 1996; Carroll & Kopf 2007).

This Letter is devoted to employing Stokes *V* asymmetry in order to diagnose the internal structure of network magnetic features, i.e., the strongest flux accumulations in the quiet Sun. Since the work of Stenflo (1973) we have known that network patches are composed of magnetic elements with kG fields. Later, two very different models were proposed to explain the observed asymmetries. The thin flux-tube model assumes a rather vertical magnetic tube expanding with height. The MISMA hypothesis assumes an infinite number of magnetic atmospheres in the resolution element. In both cases, the cause for the asymmetries is the correlation between the distribution of magnetic fields and velocities. However, the MISMA model is a one-dimensional model, having no predictive power for the spatial variation of asymmetries in magnetic structures. In order to understand how magnetic fields are really organized and to discern between these two models (or create new ones), we must observe at higher spatial resolutions, which will allow us to directly map the substructure of magnetic features and to trace gradients along the optical depth.

## 2. DATA AND ANALYSIS

We map the Stokes *V* profile asymmetries in the quiet Sun using data obtained by IMaX (Martínez Pillet et al. 2011) on Sunrise (Solanki et al. 2010; Barthol et al. 2011). The data analyzed here consist of Stokes *I* and *V* profiles of the Fe I 5250.2 Å line (Landé factor of 3) sampled at 11 wavelength positions that were recorded on June 10 at the disk center. The effective field of view (FOV) is 46.″8 × 46.″8 and the spatial resolution is about 0.″2. The noise level in Stokes *V* is $10^{-3}$ in units of the continuum intensity, $I_c$, prior to the application of the phase-diversity reconstruction technique. After this procedure, the noise of the reconstructed data is spatially and temporally correlated, but still follows a Gaussian distribution, with a standard deviation of $2.5 \times 10^{-3}\ I_c$.

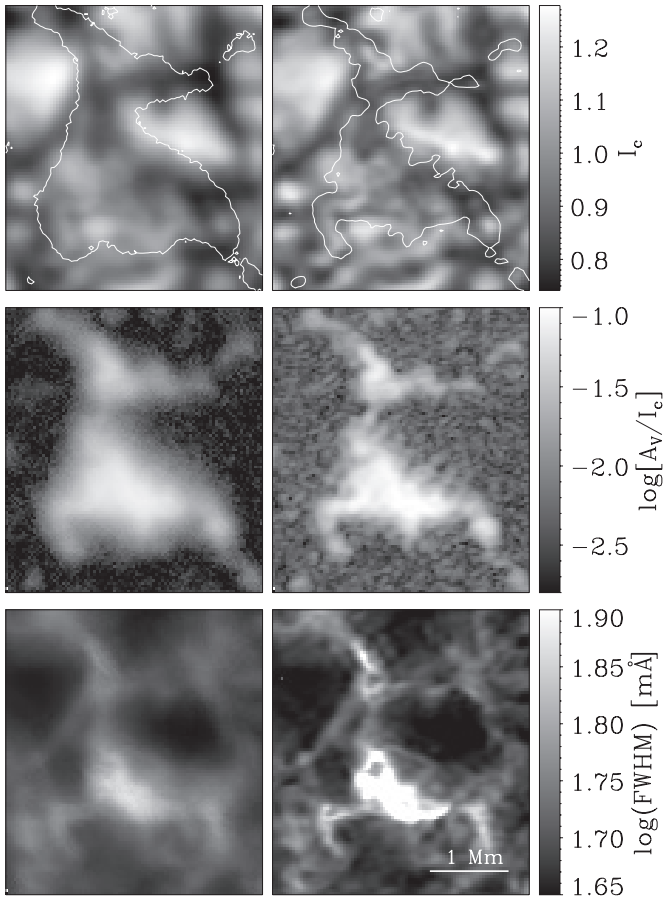


**Figure 1.** From top to bottom, continuum intensity, circular polarization amplitude, and FWHM of the intensity profile for the strongest flux region in the IMaX field of view. Left panels display the observables of the original data, while the right ones show the same scenes after phase-diversity reconstruction. The white contours represent the isocontours of $\log[A_V/I_c] = -2.3, -1.9$ for the non-reconstructed and the reconstructed data, respectively. The symbol $A_V$ represents the amplitude of the Stokes $V$ profile.

For the analysis presented in this Letter, we select a small region of the FOV containing the largest and the most intense circular polarization patch (see Figure 1). It has a magnetic flux of $\sim 2 \times 10^{19}$ Mx contained in an area of $\sim 5.5$ Mm$^2$. The pattern of the granulation is distorted within the magnetic patch, which is typical of kG field accumulations. In order to minimize the effect of the noise in our analysis, we select only those profiles with amplitudes larger than five times the noise level; 46.6% of the nonreconstructed and 29.3% of the reconstructed profiles belonging to the small selected area meet this criterion. The selected Stokes $V$ profiles in this region are mostly regular profiles. More precisely, 93.6% and 88.9% of the profiles have two lobes in the nonreconstructed and in the phase-diversity reconstructed data, respectively. We define the area ($\delta A$) and amplitude ($\delta a$) asymmetries of regular profiles as

$$\delta A = \sigma \frac{\int_{\lambda_i}^{\lambda_f} V(\lambda) d\lambda}{\int_{\lambda_i}^{\lambda_f} \mid V(\lambda) \mid d\lambda} \quad (1)$$

$$\delta a = \frac{a_b - a_r}{a_b + a_r}. \quad (2)$$

The symbols $\lambda_i = 5250.0164$ Å and $\lambda_f = 5250.4014$ Å are the initial and final wavelengths of the integral over the observed profile. The symbol $\sigma$ is the sign of the Stokes $V$ blue lobe. The $a_b$ and $a_r$ symbols are the unsigned blue and red lobe amplitudes, respectively. The nonlinearity of the equations used to compute asymmetries makes it difficult to evaluate the relevance of instrument errors. The first error source to take into account is the photon noise. We have verified (simulating Stokes $V$ profiles as derivatives of a Gaussian that match IMaX intensity data and including Gaussian noise) that the photon noise does not introduce a bias in the calculation; it only spreads the results, the relative errors in the area and amplitude asymmetries being at most $\pm 15\%$.

Calibrations performed at the launch station in Kiruna proved that considerable amounts of crosstalk exist between linear and circular polarization introduced by the ISLiD (Gandorfer et al. 2011). The relative amounts of Stokes $Q$ and Stokes $U$ change with time due to image rotation and cannot be predicted for a specific data set. When IMaX observes in a vectorial mode, all four Stokes parameters are measured and multiplication by the inverse of the Mueller matrix takes into account all crosstalk sources (leaving as unknown only the zero of the azimuth angle). In the longitudinal observing mode used here (L12-2, refer to Martínez Pillet et al. 2011) only Stokes $I$ and Stokes $V$ are measured making a proper correction of crosstalk impossible. However, we expect the impact of this crosstalk to be negligible for the investigation performed in this work which concentrates on a relatively large network patch. First of all, the fields in these regions are known to be predominantly vertical and all horizontal fields observed with IMaX in other full vector maps show that the linear polarization signals mainly corresponded to internetwork elements (Danilovic et al. 2010). Second, inspection of similar network patches observed in the IMaX vector mode V5-6 (bottom part of Figure 3 in Solanki et al. 2010) shows that they never display linear polarization signals above $3\sigma$ levels at the network concentration, either inside it or at the boundaries, where a possible canopy could generate some linear polarization. We thus conclude that in the region under study, the known crosstalk in the longitudinal mode of IMaX can be ignored even though it cannot be accounted for as is done in the IMaX vector modes.

Finally, the effect of the finite spectral (and spatial) resolution, as well as the effect of the phase-diversity reconstruction, is studied in Asensio Ramos et al. (2012) for the special case of MHD simulations. These authors conclude that the spatial degradation tends to underestimate both amplitude and area asymmetries. Degrading the spectral resolution, however, tends to overestimate the area asymmetry while it does not affect strongly the amplitude asymmetries, confirming earlier results of Solanki & Stenflo (1986). After applying the reconstruction algorithm, the computed asymmetries resemble the original ones, i.e., for MHD simulations at full spectral and spatial resolution. However, we must note that these conclusions depend on the actual shape of the profiles. The work of Solanki (1986) predicts (for the IMaX case) an overestimate of the area asymmetries by a factor of $\sim 1.6$ and an underestimate of the amplitude asymmetries by a factor of $\sim 0.8$. Consequently, strongly asymmetric/antisymmetric profiles observed by IMaX do correspond to profiles with large/small asymmetries at full spectral resolution, although the exact values may differ.

## 3. CIRCULAR POLARIZATION ASYMMETRIES AND MAGNETIC FIELD GEOMETRY

Figure 2 shows maps of the area and amplitude asymmetries of the observed Stokes $V$ profiles in the selected patch. The

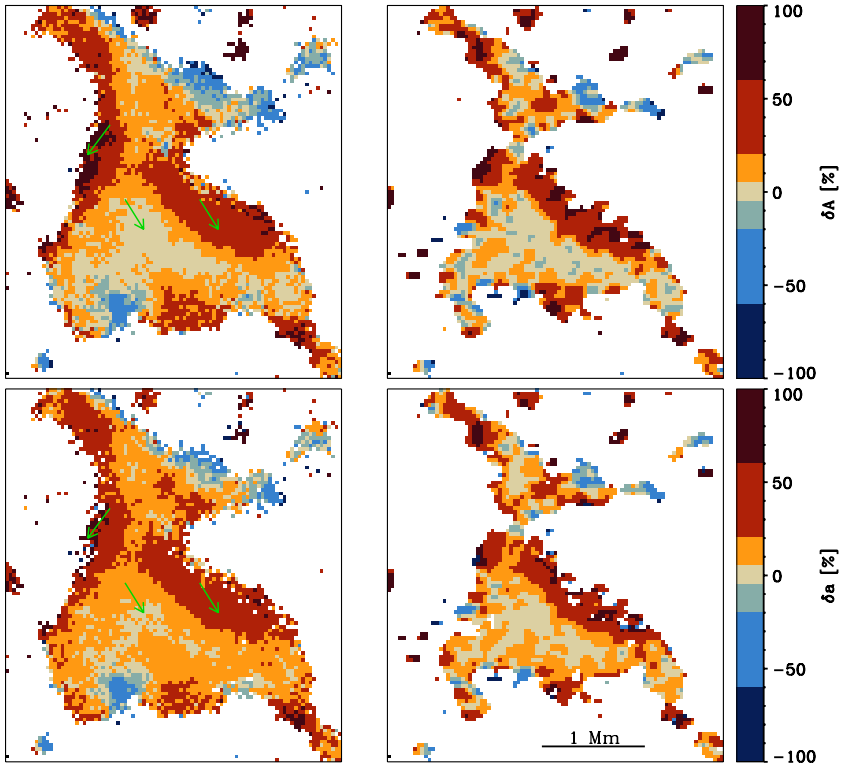


**Figure 2.** Top panels represent the area asymmetry of the circular polarization profiles of the selected strong flux patch. Bottom panels display the amplitude asymmetry. Right (left) panels present the results showing the reconstructed (nonreconstructed) data. The areas in white represent those pixels where the signal-to-noise ratio of the Stokes *V* profiles is lower than 5. Green arrows are the locations of the profiles displayed in Figure 3.

(A color version of this figure is available in the online journal.)

left panels correspond to the nonreconstructed data and the right ones to the phase-diversity reconstructed ones. All four panels display the same pattern: the smaller asymmetries tend to be located in the inner parts of the structure, while the larger ones lie at the borders close to where the signal drops below the noise level. The larger asymmetries situated at the borders of the structure have dominantly positive values, but negative values are also found (e.g., along the top edge of the feature). The spatial pattern for the two types of asymmetries is very similar, the correlation coefficient between amplitude and area asymmetries being 0.9.

Figure 3 displays three sets of Stokes *I* and *V* profiles extracted from the positions marked with small green arrows in Figure 2. The Stokes *V* profile displayed in the left panels ($\delta A = 0.5\%$ and $\delta a = 4\%$) is representative of the nearly antisymmetric profiles found in the central part of the patch. The profile in the middle panels has larger area and amplitude asymmetries (38% and 33%, respectively) as found closer to the boundary of the magnetic feature. Finally, the profile in the rightmost panels is a single-lobed profile, with extreme asymmetries: 81% area asymmetry and 80% amplitude asymmetry. Such profiles are found almost exclusively at the very edge of the feature.

In order to check if the expanding flux-tube model applies to our observations, we use the SIRJUMP code, which is a modification of the SIRGAUS code described in Bellot Rubio (2003). The two codes follow the inversion strategy of Stokes Inversion based on Response functions (SIR; Ruiz Cobo & del Toro Iniesta 1992). SIRJUMP has recently been employed to interpret single-lobed Stokes *V* profiles in the quiet Sun by Sainz Dalda et al. (2012). With SIRJUMP we retrieve the parameters of a model atmosphere showing discontinuous stratifications of some of the parameters along the line of sight. The position

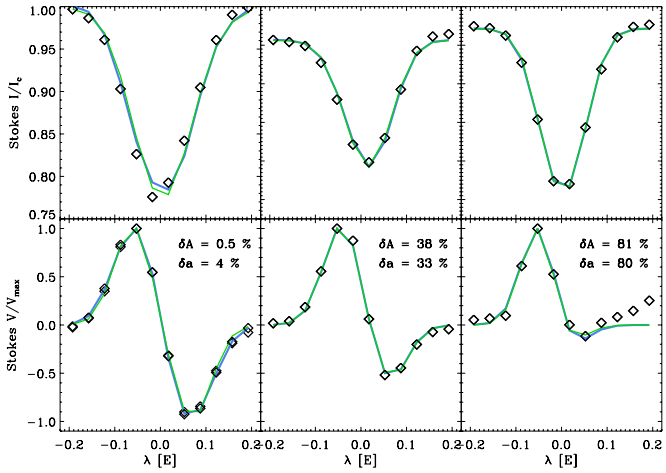


**Figure 3.** Examples of Stokes *V* profiles. The left panels display a representation of the relatively antisymmetric profiles found in the center of the structure, middle panels show the more asymmetric profiles found near the borders of the patch, and the right panels depict a single-lobed profile at the edge of the magnetic patch. The exact locations are marked in Figure 2 by small green arrows. The observed profiles are represented by the rhombs and the best fit using an inversion algorithm based on a discontinuous model along the optical depth (see the text) is displayed with a blue line. The inversion with inclination forced to zero is represented by the green lines and the inversion with the inclination as a free parameter is displayed with the blue lines.

(A color version of this figure is available in the online journal.)

of the jump (i.e., the discontinuity) is a free parameter in the inversion scheme. The code can put it below optical depth unity, which would indicate that no discontinuity is needed to explain the observed profiles. Above and below the jump, the magnetic

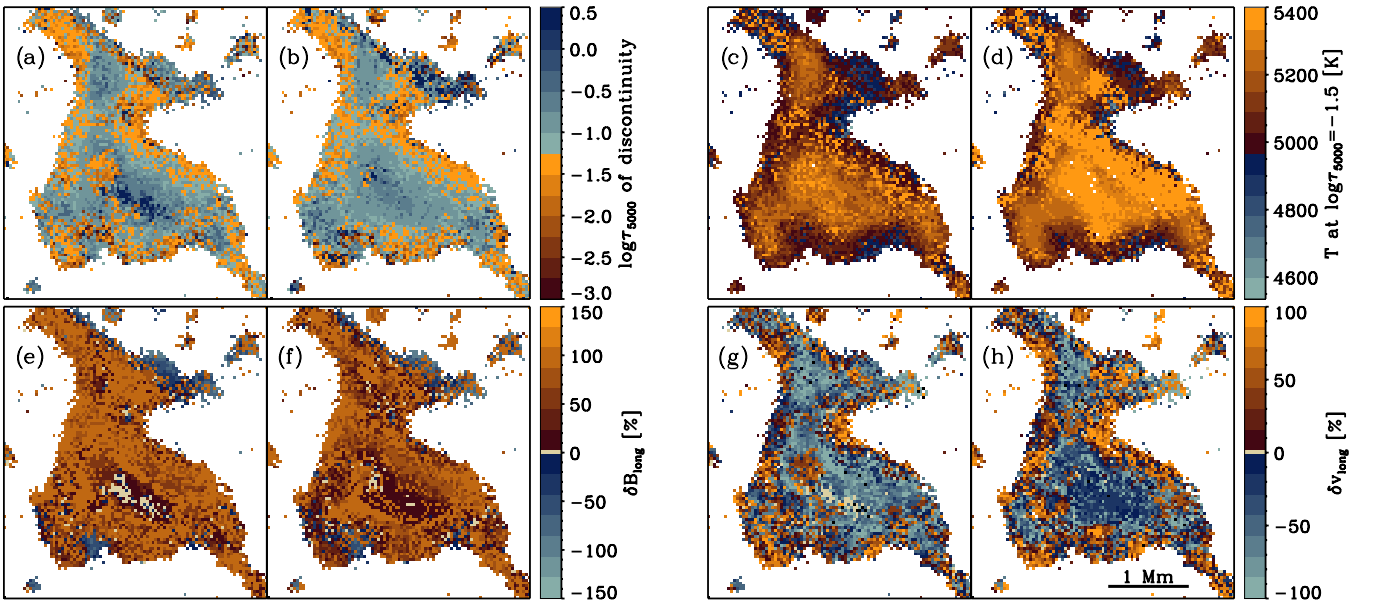


**Figure 4.** Results of the two inversions of the original data based on a model that has a discontinuity along the optical axis. Panels (a), (c), (e), and (g) display the inferred quantities for the inversion in which the inclination of the magnetic field is a free parameter. Panels (b), (d), (f), and (h) represent the retrieved parameters from the inversion in which we have fixed the inclination of the magnetic field with respect to the line of sight to 0°. Similar results can be derived from the phase-diversity reconstructed data. Panels (a)–(d) show the optical depth of the discontinuity (left) and the temperature at $\log\tau_{5000} = -1.5$ (right). Panels (e)–(h) display the relative differences of the line-of-sight magnetic field (left) and velocity (right) above and below the discontinuity (see Equation (3)).

(A color version of this figure is available in the online journal.)

field and the line-of-sight velocity are assumed to be constant with optical depth. The temperature stratification is modified with respect to an initial guess by the inversion algorithm in three nodes and interpolated between them. The microturbulent velocity and the inclination of the magnetic field vector to the line of sight are height-independent. Since we do not have information about the linear polarization, we cannot retrieve the magnetic field azimuth, and can barely infer the inclination. Therefore, we perform two different inversions, one forcing the field to be aligned with the line of sight and another one leaving the inclination as a free parameter. The macroturbulent velocity is fixed to 2.06 km s$^{-1}$, which matches the broadening induced by the point-spread function of the IMaX instrument.

Figure 4 displays the results of the two different inversions. The top left panels show the optical depth at which the discontinuity occurs for the inversion with the inclination as a free parameter (panel (a)) and the inversion forcing the inclination to 0° (panel (b)). In both cases, the results are very similar, i.e., they do not depend much on the assumed geometry of the magnetic field. For $\log\tau_{5000} \gtrsim 0.5$ the contribution to the spectral line is small and the discontinuity is not well constrained. In spite of the noise, some trends can be seen. In the central part of the structure we retrieve a magnetic field with no clear discontinuity. As we move from the center toward the edges of the structure, the discontinuity appears at increasingly higher layers. Therefore, the inversions made pixel by pixel have naturally retrieved the expansion of a magnetic flux concentration with height in the solar atmosphere. At all heights (below and above the discontinuity), the pattern of the velocity is qualitatively similar, following the local distorted granulation.

In the lower panels of the same figure we display the relative differences of the longitudinal components of the magnetic field (panels (e) and (f)) and the velocity (panels (g) and (h)) above and below the discontinuity. Note that, since we do not have linear polarization, the only trustable quantity is the longitudinal component of the magnetic field. We have used the following definitions:

$$\delta B_{\rm long} = \frac{|B^a_{\rm long}| - |B^b_{\rm long}|}{|B^a_{\rm long}| + |B^b_{\rm long}|}$$
$$\delta v_{\rm long} = \frac{|v^a_{\rm long}| - |v^b_{\rm long}|}{|v^a_{\rm long}| + |v^b_{\rm long}|}, \quad (3)$$

where the superindex $a$ and $b$ refer to the quantities above and below the discontinuity, respectively. From these figures, we can see that both the longitudinal magnetic field and the line-of-sight velocity are almost constant with optical depth at the core of the structure, coinciding with strong kG fields. As we move toward the borders of the structure (where the longitudinal component of the magnetic field is of the order of 100 G), the relative variation of both quantities increases. Note that the gradient of the longitudinal magnetic field changes sign at the regions where the area and amplitude asymmetries were negative.

## 4. CONCLUSIONS

We have computed the area and amplitude asymmetries of the Stokes $V$ profiles of the Sunrise/IMaX data set with the best spectral sampling (35 mÅ). We selected the strongest magnetic flux accumulation, which belongs to the network pattern, in the IMaX FOV. The core of the structure is, on average, characterized by an area asymmetry of 0.2% and an amplitude asymmetry of 4.4% (with an upper limit for the error of ±1.3% for both averaged area and amplitude asymmetries). In the outermost parts of the network patch, the Stokes $V$ profiles have the largest area and amplitude asymmetries, even approaching 100% (single-lobed profiles). The fact that we are seeing a spatial variation of Stokes $V$ asymmetries means that, for the first time, we are resolving the internal structure of a magnetic patch

belonging to the photospheric network. The non-negligible amplitude asymmetry inside the magnetic feature suggests that unresolved motions are still present (definitely gradients along the line of sight and probably horizontal gradients).

We inverted our data using the SIRJUMP code, which models the gradients of the magnetic field and line-of-sight velocity with an abrupt discontinuity at a certain optical depth. From two different assumptions on the inclination of the field, we inferred that the observed network patch is made of resolved kG fields which is consistent with the work of Lagg et al. (2010). Moreover, the inversions naturally retrieve a geometry corresponding to a magnetic field expanding with height.

The spatial distribution of the Stokes *V* asymmetries and the inversions applied to these data suggests a geometry similar to the classical model of magnetic features expanding with height (Spruit 1976; Solanki 1993) that takes pressure balance and magnetic flux conservation with height into account and is consistent with three-dimensional magnetohydrodynamical simulations (Yelles Chaouche et al. 2009). In such a model, the central core of the structure traces the body of the flux tube, containing the vertical kG fields, while the external parts correspond to the canopy, i.e., expanding, inclined field overlying the quiet photosphere (this expansion is caused by the need to conserve magnetic flux for decreasing gas pressure with height).

The standard model for the creation of asymmetries in the presence of such a canopy is based on the presence of a discontinuity in both the magnetic field strength and the line-of-sight velocity at the base of the canopy (i.e., abrupt gradients in such quantities along the optical depth). In the past, it was assumed that there is no velocity flow above the canopy's base but there is a downflow below it, with the magnetic field being present only above the canopy base. This geometry produced a positive area (and amplitude) asymmetry (Grossmann-Doerth et al. 1988; Solanki 1989), with nearly single-lobed profiles in the outer parts of the flux tubes (Solanki 1989) in agreement with the observations.

Our results for the asymmetries (see Figure 2) are in agreement with this general picture. However, there are some locations along the edge of our feature where the area (and amplitude) asymmetry is negative, indicating that either the magnetic field or the velocity field gradient must change sign there. We know that the kG network fields are embedded in the more disorganized weakly magnetized quiet photosphere. Hence, we would expect a smooth transition between the organized kG fields to the tangled weak photospheric fields (note that we have selected the profiles above the noise level, i.e., the borders of the structure depend on the amplitude required for the profiles). If those regions are mostly tracing the quiet photosphere (note that the height of the discontinuity is located at lower layers and that the temperature is colder than that of the central part of the structure), it is not surprising to find gradients of magnetic field and velocity that change sign as compared to the classical canopy overlying a nonmagnetized photosphere.

The observations presented in this Letter support the interpretation of the network as kG fields expanding with height. In contrast to what was assumed in the past, we find velocity patterns above and below the canopy that follow the local distorted granulation. To strengthen the model for strong flux concentrations such as the one studied in this Letter, in the future we need to include in our analysis the constraints introduced by the linear polarization and, more importantly, the simultaneous information of many spectral lines to trace the canopy at different heights.

We especially thank Manuel Collados Vera for very helpful discussions and for carefully reading the manuscript. The Spanish contribution has been funded by the Spanish Ministry of Science and Innovation under projects ESP2006-13030-C06, AYA2009-14105-C06 (including European FEDER funds), and AYA2010-18029 (Solar Magnetism and Astrophysical Spectropolarimetry). The German contribution to Sunrise is funded by the Bundesministerium für Wirtschaft und Technologie through Deutsches Zentrum für Luft- und Raumfahrt e.V. (DLR), grant No. 50 OU 0401, and by the Innovation fund of the President of the Max Planck Society (MPG). This work has been partially supported by the WCU grant (No. R31-10016) funded by the Korean Ministry of Education, Science, and Technology.

## REFERENCES

Asensio Ramos, A., Martínez González, M. J., Khomenko, E., & Martínez Pillet, V. 2012, A&A, 539, 42
Barthol, P., Gandorfer, A., Solanki, S. K., et al. 2011, Sol. Phys., 268, 1
Bellot Rubio, L. R. 2003, in ASP Conf. Ser. 307, Solar Polarization, ed. J. Trujillo-Bueno & J. Sanchez Almeida (San Francisco, CA: ASP), 301
Bellot Rubio, L. R., Ruiz Cobo, B., & Collados, M. 1997a, ApJ, 478, 45
Bellot Rubio, L. R., Ruiz Cobo, B., & Collados, M. 1997b, ApJ, 478, 47
Bünte, M., Darconza, G., & Solanki, S. K. 1993, A&A, 274, 478
Carroll, T. A., & Kopf, M. 2007, A&A, 468, 323
Danilovic, S., Beeck, B., Pietarila, A., et al. 2010, ApJ, 723, L149
Gandorfer, A., Grauf, B., Barthol, P., et al. 2011, Sol. Phys., 268, 35
Grossmann-Doerth, U., Keller, C. U., & Schüssler, M. 1996, A&A, 315, 610
Grossmann-Doerth, U., Schüssler, M., & Ssolanki, S. K. 1988, A&A, 206, 37
Illing, R. M. E., Landman, D. A., & Mickey, D. L. 1975, A&A, 41, 183
Lagg, A., Solanki, S. K., Riethmüller, T. L., et al. 2010, ApJ, 723, L164
López Ariste, A. 2002, ApJ, 564, 379
Martínez González, M. J., Collados, M., Ruiz Cobo, B., & Beck, C. 2008, A&A, 477, 953
Martínez Pillet, V., Del Toro Iniesta, J. C., Álvarez-Herrero, A., et al. 2011, Sol. Phys., 268, 57
Martínez Pillet, V., Lites, B. W., & Skumanich, A. 1997, ApJ, 474, 810
Rezaei, R., Steiner, O., Wedemeyer-Böhm, S., et al. 2007, A&A, 476, L33
Ruiz Cobo, B., & del Toro Iniesta, J. C. 1992, ApJ, 398, 375
Sainz Dalda, A., Martínez-Sykora, J., Bellot Rubio, L., & Title, A. 2012, ApJ, 748, 38
Sánchez Almeida, J., Collados, M., & del Toro Iniesta, J. C. 1989, A&A, 222, 311
Sánchez Almeida, J., & Landi Degl'Innocenti, E. 1996, Sol. Phys., 164, 203
Sigwarth, M. 2000, Rev. Mod. Astron., 13, 45
Sigwarth, M. 2001, ApJ, 563, 1031
Solanki, S. K. 1986, A&A, 168, 311
Solanki, S. K. 1989, A&A, 224, 225
Solanki, S. K. 1993, Space Sci. Rev., 63, 1
Solanki, S. K., Barthol, P., Danilovic, S., et al. 2010, ApJ, 723, L127
Solanki, S. K., & Stenflo, J. O. 1984, A&A, 140, 185
Solanki, S. K., & Stenflo, J. O. 1986, A&A, 170, 120
Spruit, H. C. 1976, Sol. Phys., 50, 269
Stenflo, J. O. 1973, Sol. Phys., 32, 41
Stenflo, J. O., Solanki, S. K., & Harvey, J. W. 1987, A&A, 171, 305
Viticchié, B., & Sánchez Almeida, J. 2011, A&A, 530, 14
Yelles Chaouche, L., Solanki, S. K., & Schüssler, M. 2009, A&A, 504, 595